Journal of Physics D:
Applied Physics

PAPER • **OPEN ACCESS**

SPPARK—a novel generalized simulation tool for non-equilibrium plasma chemistry

To cite this article: Andrea Marchetti *et al* 2025 *J. Phys. D: Appl. Phys.* **58** 315204

OPEN ACCESS
IOP Publishing
Journal of Physics D: Applied Physics
J. Phys. D: Appl. Phys. **58** (2025) 315204 (13pp)
https://doi.org/10.1088/1361-6463/adeb98

SPPARK—a novel generalized simulation tool for non-equilibrium plasma chemistry

Andrea Marchetti[1,*], **Romolo Laurita**[1] and **Matteo Gherardi**[1,2]

[1] Department of Industrial Engineering, Alma Mater Studiorum, Università di Bologna, Bologna, Italy
[2] Advanced Mechanics and Materials, Interdepartmental Center for Industrial Research (AMM-ICIR), Alma Mater Studiorum, Università di Bologna, Bologna, Italy

E-mail: andrea.marchetti18@unibo.it

Received 28 April 2025, revised 27 June 2025
Accepted for publication 3 July 2025
Published 4 August 2025

Abstract

Plasma applications in the chemical industry are gaining interest due to the possibility of improving the environmental sustainability of chemical processes in their electrification scenario while also favoring their circularity. To allow the possibility of an in-depth understanding of the fundamental chemical mechanisms, zero-dimensional plasma-chemistry numerical models are often adopted to simulate the time evolution of plasma-gas systems. To increase the physical representativeness of numerical models a novel, fully customizable, plasma chemistry solver simulation platform for plasma assisted reactive kinetics has been developed by runtime coupling Cantera (dealing with the rigorous time integration of the chemical ordinary differential equation system) to Bolsig+ (dealing with the detailed description of electron kinetics). A complete description of its modeling capabilities is here presented together with the validation results obtained by the comparison against the state-of-the-art solver ZDPlasKin.

Keywords: plasma-chemistry, non-equilibrium plasma, modeling, Cantera, Bolsig+

1. Introduction

In the context of global climate crisis, the interest towards environmental sustainability of chemical processes is arising. To reduce the industry impact on greenhouse gasses (GHGs) production, plasma technologies have demonstrated to be a possible path for the chemical industry electrification, inducing a large interest in the scientific community. Some examples of the most studied plasma-chemical processes are: methane pyrolysis to split CH4 and produce hydrogen and various carbon allotropic forms and nanostructures [1–7], low temperature methane oxidation to decrease the GHGs emissions [8–11]; methane coupling with the aim of C2 and C3 hydrocarbons production [12–17], nitrogen fixation for ammonia and fertilizers synthesis [18–25], carbon dioxide splitting [26–33], ammonia cracking [34–37] and carbon dioxide hydrogenation [38–43].

In a plasma, electrical power is coupled with the gas particles thanks to the charged particles susceptibility to electro-magnetic fields. Due to their low inertia, most of the energy is acquired by electrons and part of it is ceded to the gas (heavy) particles through collisions. Whenever the number of collisions per unit time is not high enough to thermally equilibrate electrons and heavy particles, the plasma is in non-equilibrium (i.e. a single temperature is not sufficient to describe the energies in the system). This characteristic is

* Author to whom any correspondence should be addressed.

particularly interesting in chemical processes. In fact, it allows new reaction pathways to occur that otherwise would not be relevant at equal gas temperatures [44]. Moreover, plasma-chemical processes may present fast gas temperature raises as the system proceeds toward equilibrium [45, 46].

On the other hand, these characteristics grant plasma-chemical interaction mechanisms high complexity: a large number of reactive species are coexisting in the system; the chemical kinetics is characterized by multiple timescales; the phenomena are presenting a multiphysics nature. This often leads to the need of numerical models to achieve insights on the founding mechanisms of the process.

In this context, a plasma chemistry solver is a numerical solver focusing on the zero-dimensional (0D) time-dependent evolution of the chemical system. Its general structure includes an ordinary differential equation (ODE) solver coupled with a Boltzmann solver, which is a numerical solver for the electron Boltzmann equation (EBE). The purpose of the ODE solver is to determine the time evolution of variables of interest. Concurrently, the Boltzmann solver computes the kinetic energy distribution of the electron population (electron energy distribution function—EEDF). This distribution is used to determine the electron population properties that are influencing the overall chemical kinetics. Among the available Boltzmann solvers, Bolsig+ [47] is one of the most used, granting high customization of the hypothesis influencing electron kinetic modeling. Bolsig+ is actively coupled with different ODE solvers in most of the plasma-chemistry solvers [48–52] through embedded versions limiting the model customizability.

Some of the models, for example the one adopted by ZDPlasKin [48] and Plasimo [49], are more focused on the pure non-equilibrium plasma phenomena description. In fact, they allow users to include non-equilibrium reaction rate constants (i.e. dependent on the temperature, drift velocity or diffusivity of electrons), to use signals of electrical power densities coupled to the plasma directly as an electron solicitation (through power coupling models) for the EBE solution and to decouple the collisions utilized in the Boltzmann solver from the ones included as chemical reactions in the ODE solver. On the other hand, these kinds of solvers lack chemical model customizability as they are generally limited to perfectly stirred reactor (PSR) models with a poor description of the reaction thermodynamics of the system as they may require users to define a constant value of reaction enthalpy for each reaction.

On the other hand, some plasma-chemistry solvers are being developed based on more complex thermochemical solvers [50, 51]. One of the most used is Cantera [53], a freeware open-source code highly used in the chemistry modeling community, making use of its rigorous system thermodynamic modeling and customizability. From the reaction thermodynamics perspective, Cantera offers the possibility to include species thermodynamic properties as functions of the gas temperature, thus influencing the heat release (or absorbtion) from reactions during the computations. The plasma-chemistry solvers based on Cantera include a Boltzmann solver, e.g. BOLOS [50] and its C++ version CppBOLOS [51], to manage the electron collisional processes but are not including custom defined non-equilibrium reactions nor power coupling models to input power density signals to the EBE solver.

To enlarge the physical representativeness of plasma-chemistry models, a novel solver, simulation platform for plasma assisted reactive kinetics (SPPARK), has been developed by the Authors based on a Cantera—Bolsig+ coupling. The coupling aim is granting chemical rigorousness and flexibility of application together with full customizability of the physical hypothesis influencing the EBE solution with the objective of filling the gaps between the two families of plasma-chemistry solvers, providing researchers with an open-source environment to simulate complex plasma-chemical processes. In this sense, SPPARK is able to: include electron collision processes in Cantera chemistry sets; include non-equilibrium reactions with arbitrary complex reaction rate constants; make use of power coupling models or electric circuit schemes to extract the electron solicitation to feed Bolsig+ with; deal with heterogeneous plasma–gas mixtures; include multizone modeling of plasma sources; use the formulations available in Cantera to represent the species thermodynamic properties as a function of gas temperature.

The present work describes the SPPARK solver, the plasma-chemistry models currently included, and the methodology adopted for Cantera–Bolsig+ coupling. A validation of the software is also presented comparing SPPARK computations against data obtained with the widely adopted ZDPlaskin [48] code using reaction mechanisms describing a N_2 plasma and an Ar plasma under multiple operating conditions. Moreover a simple CH_4 splitting model is included to further argue on the necessity including a rigorous thermodynamic representation of the system for applications with large ranges of temperature variability.

2. Model description

A plasma-chemistry model aims to the detailed representation of the chemical mechanisms that occur in a plasma. The goal can be reached by describing the phenomena existing in the plasma discharge and the effects that these have on the state of the gas. First of all, electron collisions should be included in the model as they allow energy to be transferred from electrons to heavy particles. These collisions, together with the electromagnetic field intensity, are responsible for the overall behavior of the electron population as a swarm of particles (i.e. their mean energy $\langle\varepsilon\rangle$, their diffusion coefficient D_e, their mobility coefficient μ etc.). Through collisions, which are considered as chemical reactions, electrons can drive energy to the mean kinetic energy of the gas particles (their temperature) or to their internal energy (i.e. exciting their electronic state). Species produced by electron collisions are reacting in the gas system. As these particles state is shifted from the

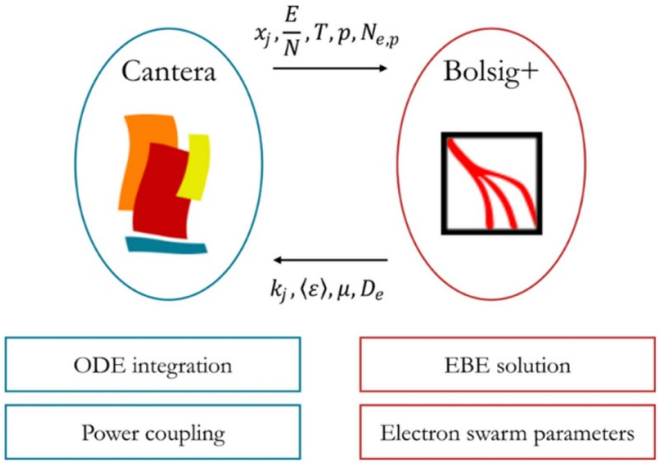

Figure 1. Cantera-Bolsig+ coupling conceptual scheme. Boxed are represented the specific tasks attributed to each solver. Arrows indicate the data transfer between the two: the system thermodynamic state and electron solicitation from Cantera to Bolsig+ and the electron swarm parameters from Bolsig+ to Cantera.

macroscopic equilibrium (i.e. the equilibrium state defined by the gas temperature in low ionization plasmas), the rates of the reactions they are involved in are generally a function of the overall plasma state (i.e. are also dependent on the electron swarm coefficients) and so cannot be analytically expressed through simple Arrhenius rate constants. All of these aspects are addressed in SPPARK through the Cantera–Bolsig+ coupling rationale schematically represented in figure 1.

The coupling involves Bolsig+ to solve the EBE, obtaining the EEDF from which the electron collisions rates (k_j) and the kinetics parameters can be derived, and Cantera to compute the electron solicitation for Bolsig+ through power coupling models and to time integrate the ODEs to obtain the new plasma state (its temperature T, pressure p, molar fraction x_j and electron density $N_{e,p}$) at each timestep.

In this section, the theoretical model representing electron collisions, non-equilibrium processes, power coupling models, electron effects on gas temperature and heterogeneous plasma interactions are described. Furthermore, the adopted strategies to include electron collisions and non-equilibrium reactions in objects derived from Cantera classes together with the methodology of synchronized coupling of Bolsig+ during the time integration are introduced.

2.1. Plasma chemical kinetics

Electron collisions are the driving force of the non-equilibrium chemical processes taking place in a plasma. In general, electron collisions are considered as binary reactions with the heavy species being targeted by the impact assumed to be stationary [54]. By convention, collisions can be classified as: elastic when the energy ceded by the colliding electron is conveyed in the kinetic energy of the heavy target particles; inelastic when the energy transfer from the electron results in a variation of the internal energy of the target particle. Macroscopically, elastic collisions lead directly to a raise of the gas temperature whilst the inelastic collisions in the production of new chemical compounds (generally unstable); these can be electronically excited states of a species, rotovibrationally excited states of molecules, ions and radicals. Each of the produced species will then interact with the whole system of particles resulting in a superposition of thermochemical, electron kinetics and non-equilibrium mechanisms. The last two reaction mechanisms require the definition of rate constants (k_j).

Electron collisions rate constants are obtained directly from their cross-section by the following integral formulation:

$$k_j^{\mathrm{coll},f} = \gamma \int_0^\infty \varepsilon \sigma_j(\varepsilon) F(\varepsilon)\, \mathrm{d}\varepsilon \tag{1}$$

where, $\sigma_j(\varepsilon)$ (m^2) represents the cross-section of the jth collision, $F(\varepsilon)$ $\left(eV^{-3/2}\right)$ the EEDF, ε (eV) the kinetic energy of the colliding electron and $\gamma = \left(\frac{2e}{m_e}\right)^{1/2}$ a constant with e (C) and m_e (kg) electron charge and mass respectively. In case of reversible reactions, the inverse rate constant is determined through the following expression [47],

$$k_j^{\mathrm{coll},i} = \frac{g_h}{g_l} \cdot \gamma \int_0^\infty (\varepsilon - U_j) \sigma_j(\varepsilon - U_j) F(\varepsilon)\, \mathrm{d}\varepsilon \tag{2}$$

where $\frac{g_h}{g_l}$ is the statistical weight ratio between the forward collision products (g_h) and the forward collision reactants (g_l) and U_j (eV) is the threshold energy of the collision.

The EEDF can be obtained by solving the EBE [47]:

$$\frac{\partial f}{\partial t} + \vec{v} \cdot \nabla f - \frac{e}{m_e} \vec{E} \cdot \nabla_v f = C \tag{3}$$

where f is the electron distribution in the six-dimensional phase space, $\vec{x}$ and $\vec{v}$ are respectively the vector of space and velocity coordinates, $\vec{E}$ is the electric field and C is the collision integral term of the equation.

On the other hand, the non-equilibrium reactions rate constants are usually expressed in analytical formulations depending on both the gas overall thermodynamic state and electron kinetic parameters (*i.e.* electron temperature, mobility and diffusion coefficients) also obtained from the EEDF [47]:

$$k_j^{\mathrm{neq}} = k_j^{\mathrm{neq}}(T_{\mathrm{gas}},\, T_e,\, \mu_e,\, D_e, \ldots). \tag{4}$$

2.2. Power coupling models

As described in [47], the external solicitation required for the EEDF equation solution is the reduced electric field E/N (with E electric field magnitude and N heavy particles number density). In general, the reduced electric field is laboriously measured, thus, to extend experimental data availability, deposited power density values are more often used as the electron solicitation [3, 55, 56]. For this reason, to solve

the EEDF equation, which explicitly depends on the reduced electric field value [47], using the deposited power density, a correspondence between power densities and reduced electric fields values is required. This is obtained through power coupling models. Among the available ones, two are here described. The first algebraic model utilizes the local field approximation (LFA) [54] to obtain $E/N\,(Td)$ directly from the deposited power density:

$$\frac{E}{N} = \frac{1}{N}\sqrt{\frac{\tilde{P}_p}{N_{\mathrm{e,p}} e \mu_e}} \cdot 10^{21} \tag{5}$$

where N is the heavy particles number density (m^{-3}), $\tilde{P}_p$ is the deposited power density in the plasma ($\mathrm{W\,m}^{-3}$), $N_{\mathrm{e,p}}$ is the electron number density (m^{-3}) in the plasma and μ_{e} is the electron mobility ($\mathrm{m}^2/(\mathrm{V}\cdot\mathrm{s})$). This relation is obtained by the Joule heating equation:

$$\tilde{P}_p = \sigma E^2 \tag{6}$$

where the approximation $\sigma \approx N_{\mathrm{e,p}} e \mu_{\mathrm{e}}$ is introduced making the whole power coupling model hold for low excitation frequencies [54].

The second model is generally more accurate as it relies on the homogeneous local mean energy approximation (LEA) [57] from which the following equation can be obtained and solved to compute the mean electron energy ($\langle\varepsilon\rangle - eV$):

$$\frac{\mathrm{d}\langle\varepsilon\rangle}{\mathrm{d}t} = \frac{1}{N_{\mathrm{e,p}}}\left(\frac{\tilde{P}_{\mathrm{p}}}{e} - Q_{\mathrm{el}} - Q_{\mathrm{in}} - \langle\varepsilon\rangle\frac{\mathrm{d}N_{\mathrm{e,p}}}{\mathrm{d}t}\right) \tag{7}$$

where Q_{el} and Q_{in} are the powers deposited (lost) by electrons respectively in elastic and inelastic collisions ($\mathrm{eV\,s}^{-1}$). Both Q_{el} and Q_{in} can be computed from the EEDF [47] as follows:

$$Q_{\mathrm{el}} = N_{\mathrm{e,p}} N \sum_{j=\mathrm{elastic}} \gamma x_j \frac{2\mathrm{m}_e}{M_j} \int_0^\infty \left[\sigma_j\left(\varepsilon^2 F + \frac{K_b T}{e}\frac{\partial F}{\partial \varepsilon}\right)\right]\mathrm{d}\varepsilon \tag{8}$$

$$Q_{\mathrm{in}} = N_{\mathrm{e,p}} N \sum_{j=\mathrm{inel}} U_j x_j \left(y_j^{\mathrm{low}} k_j^{\mathrm{coll},f} - y_j^{\mathrm{up}} k_j^{\mathrm{coll},i}\right) \tag{9}$$

where x_j and M_j are respectively the molar fraction (considering just the heavy particles) and the mass (kg) of the chemical species involved in the jth collision, K_{b} the Boltzmann constant ($\mathrm{J\,K}^{-1}$), T the gas temperature, U_j the energy threshold of the jth collision (*i.e.* the chemical bond energy for a dissociation, the energy gap between two electronic shells, etc…) and y_j^{low} and y_j^{up} the population fractions in the lower and upper excited states. The E/N value is then obtained by matching mean electron energy obtained by equation (7) with the one obtained by [47]:

$$\langle\varepsilon\rangle = \int_0^\infty \varepsilon^{\frac{3}{2}} F(\varepsilon)\,\mathrm{d}\varepsilon \tag{10}$$

with F being obtained by the solution of the EEDF equation with the target E/N value as an input.

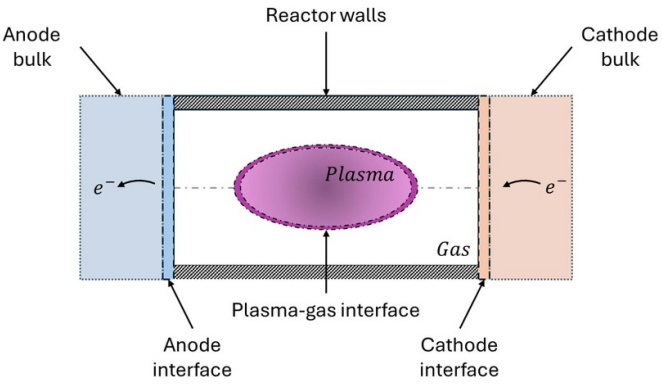

Figure 2. Abstract representation of a plasma reactor including walls, electrodes and plasma-gas interfaces.

2.3. Heterogeneous phase plasma interactions

In many systems the generated plasma phase is in contact with electrodes and reactor walls. For this reason, including heterogeneous phase plasma–solid interaction is fundamental to comprise the additional charged particles losses. Moreover, many plasma discharges cannot be considered to be homogeneous, being characterized by an admixture of gas and plasma phases (figure 2). The plasma–boundary interactions and plasma-gas mixtures models adopted by the Authors are here described.

2.3.1 Plasma-boundary interactions. Heterogeneous plasma–solid interactions can be described by means of surface interactions at the interfaces between the plasma and the solid phases. These interfaces can be represented as catalytic solid interfaces being characterized by an area (A) and a density of active sites (S_{d}). In addition, the loss mechanisms can be included as surface reactions occurring on the surface of the catalyst. The here presented model refers to two types of plasma-solid interfaces: *Walls* and *Electrodes*. *Wall* interfaces allow species to stick to their surfaces introducing additional loss terms for the species interacting with them. On the other hand, *Electrode* interfaces are characterized by permeability to electrons. A solid phase must then be included to function as a reservoir of solid electrons to be ceded (in a cathode electrode) or to be extracted (in an anode electrode) from the *Electrode* interfaces. The plasma solid interactions are particularly relevant to include charged particles losses to the system boundaries. The model adopted by the Authors allows to consider these losses through the definition of a transport loss frequencies (ν_{L}) and to determine the loss rate constant; in the following example, a general mechanism of electron loss to an anode interface (represented by an anode active site $A\,(S)$) is presented,

$$\begin{cases} e^- + A\,(S) \overset{k_0}{\Rightarrow} A(S)^- \overset{k_1}{\Rightarrow} A\,(S) + e^-_{\mathrm{anode}} \\ k_0 = \nu_{\mathrm{L}} \cdot \frac{V}{A} \cdot \frac{1}{S_{\mathrm{d}}} \\ k_1 = k_1 \gg k_0 \end{cases} . \tag{11}$$

In the above expression k_0 represents the plasma-to-surface loss mechanism rate constant, whilst k_1 represents the anode restoration rate constant with V being the plasma volume. The k_1 constant is arbitrarily chosen to be much greater than k_0 to ensure the instantaneous restoration of the active sites of the electrode.

Many expressions to include charged particles transport losses ν_L in 0D plasma-chemistry modeling have been presented by Alves and Tejero-del-caz depending on the dominant discharge phenomena [58].

2.3.2 Plasma-gas mixtures. To extend the applicability of the model to non-homogeneous plasma discharges two approaches are here introduced. The first one makes use of the same principle used for plasma-solid interactions. If a plasma-gas interface can be properly defined, the transport of species between the two phases can be modeled introducing a fictitious surface of voids ($V(S)$). Doing so, a transport frequency (ν_τ) can be used to model the exchanges between the two phases as in the following example:

$$\begin{cases} X^{(p)} + V(S) \underset{k_1}{\overset{k_0}{\Leftrightarrow}} V(S) + X^{(g)} \\ k_0 = \nu_\tau^{(p)} \cdot \frac{V_p}{A} \cdot \frac{1}{S_d} \\ k_1 = \nu_\tau^{(g)} \cdot \frac{V_g}{A} \cdot \frac{1}{S_d} \end{cases} \tag{12}$$

with k_0 being the plasma-to-gas transport rate constant, k_1 the gas-to-plasma one and $X^{(p)}$, $X^{(g)}$ referring to the same X species considered in the plasma and gas phase respectively. V_p and V_g here represent the plasma and gas phases volumes respectively whilst $\nu_\tau^{(p)}$ and $\nu_\tau^{(g)}$ the plasma-to-gas and gas-to-plasma transport frequencies.

If the plasma–gas interface cannot be easily defined (*i.e.* the two phases are strongly mixed), a second approach can be used by introducing a volume weighted approximation. Assuming that free electrons are present only in the homogeneous plasma phase, the EBE can be solved by considering a higher density electron population obtained by the global (mean) electron density as:

$$N_{e,p} = \frac{N_e}{\varphi} \tag{13}$$

where N_e is the electron number density in the whole volume and the term $\varphi = \frac{V_p}{V_{tot}}$, with V_p the plasma volume and V_{tot} the total volume, is the plasma to total volume ratio. Under this approximation, the collisions rate constants and electron kinetic parameters are calculated as in a pure-plasma homogeneous system, but their overall effect is downscaled by considering an available population of N_e particles to be able to support the non-equilibrium processes.

2.4. Implementation in Cantera

The previous sections highlighted the need of a closed coupling between Cantera and Bolsig as summarized in figure 3.

Bolsig+ is freely available as an executable file. Its command line operated version elaborates the user requests delivered in a text file. The input file contains the hypothesis on the electron kinetics model, the path to the cross-section data file and the path to the output text file. To couple Cantera and Bolsig+ in a python environment, a python wrapper to write the inputs, execute the simulation and read the results has been developed. To ensure the consistency of the electron kinetic simulation with the plasma-gas system state the wrapper consists of a system of python classes representing species, reactions and the whole particles system which allows the runtime coupling of the two codes.

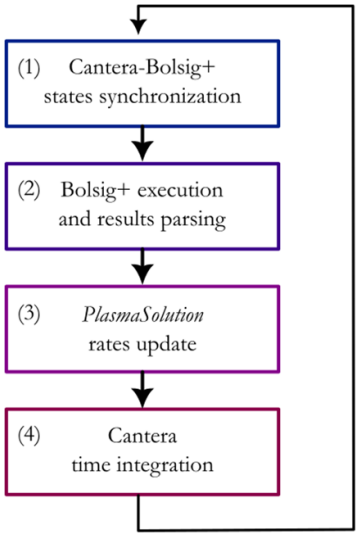

Figure 3. Single time-step Cantera–Bolsig+ coupling algorithm. At the beginning of the time-step the Bolsig+ gas state is synchronized (1) accordingly with the results obtained by Cantera in the ODE time integration together with the reduced electric field value relative to the simulation time (either imposed or computed by the power coupling model of choice). Bolsig+ is then called (2) to solve the electron Boltzmann equation and extract the electron transport and kinetic parameters which are parsed and fed back to the PlasmaSolution object (3) to update the rate reaction constants. Ultimately, the time integration of the ODEs at the current simulation time is effectuated (4) providing the results necessary for the new time-step.

In SPPARK the single timestep operations are executed as follows and summarized in figure 3: at first a synchronization of the Bolsig+ hypothesis to a *PlasmaSolution* (the SPPARK *Solution* class inheriting its attributes and methods from the Cantera *Solution* class) state is performed; secondly, a call of Bolsig+ computes the electron collisions rates and the electron kinetics parameters for the non-equilibrium reaction rates, which are parsed from the Bolsig+ output text file; non-equilibrium rates are computed and the numerical values of electron collisions and non-equilibrium rate constants are updated in the *PlasmaSolution* object; afterwards the time integration in Cantera is carried out obtaining a new state for the *PlasmaSolution* object allowing the next timestep to occur. The runtime coupling of the two solvers is obtained through the *ExtensibleReactor* classes available in Cantera by modifying the constitutive equations to consider the plasma effects on the system.

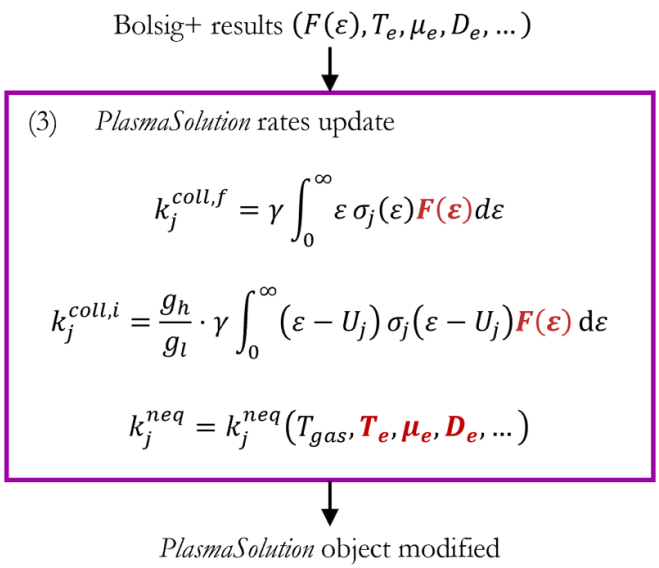

Figure 4. Detailed description of the Bolsig+ results coupling to reaction rate constants. The terms highlighted in red are results directly parsed from the Bolsig+ output files which are used in the *after_get_state* method of the *ExtensibleReactor* class of Cantera to modify the rate constants of electron collisions and non-equilibrium reactions.

Depending on the application, users can select the *ExtensibleReactor* of choice and apply the same coupling procedure previously described.

To further clarify the procedures required to consider electron collisions and non-equilibrium reactions in Cantera, represented by point (3) in figure 3, figure 4 provides an in-depth scheme of the rate constants update. These operations are executed in the *after_get_state* method of the *ExtensibleReactor* class before the evaluation of the ODEs terms is performed in its *after_eval* method.

2.4.1. Plasma chemical kinetics. The electron collision rate constants computation requires the integration of the cross-section of the reaction weighted on the EEDF, as described in equation (1). Concurrently, non-equilibrium reactions are strongly dependent on the electron kinetic parameters. In Cantera the definition of user defined rate constants is implemented by the use of *CustomRate* and *ExtensibleRate* classes. The first one presents a strong limitation since it allows the definition of a custom function for the rate computation only dependent on the gas temperature. The other can take all the thermodynamic data from a *Solution* object and use it to evaluate the rate. Although the latter is a positive feature, the implementation of a new rate requires a new class definition for each additional reaction, which is not suitable for large chemistry sets. By virtue of these considerations, two different approaches have been applied for electron collisions and non-equilibrium reactions. The first are treated as constant Arrhenius rates whose values are updated each timestep using the results obtained from Bolsig +. For this reason, the reactions are first defined through the cross-section data in the Bolsig+ input text file and then coupled to Cantera *Reaction* objects. Additionally, users can selectively choose which subset of the electron collisions used in Bolsig+ to compute the EEDF to include in the ODE time integration. For the second type of reactions, the customized class *CustomPlasmaReaction* is introduced. This class takes the reaction equation, a reaction order and a python function as inputs. The python function is user defined and returns the rate constant value. Each instance of this class is then associated with a Cantera *Reaction* object in a *PlasmaSolution* object whose rate is updated at each timestep. Furthermore, electron inelastic collisions and some non-equilibrium reactions (*i.e.* some radiative relaxations of electronically excited species) should not directly influence the gas temperature computation. For this reason, all the inelastic collisions and the subset of *CustomPlasmaReaction* objects are extracted in the *PlasmaSolution* class as no-heat reactions, whose reaction enthalpy will not be considered in the heat equation.

2.4.2. Power coupling models. To include the two power coupling models (equations (5) and (7)) in the runtime coupling, they have been introduced in two *ExtensibleReactor* classes. The LFA model (5) is simply included in the *after_get_state* method of the class whilst the LEA model (7) is included in its *after_eval* method.

2.4.3. Heterogeneous plasma interactions. To ensure the maximum freedom in modeling transport phenomena, an additional *PlasmaInterface* class (inheriting from the Cantera *Interface* class) has been introduced. The class has the possibility of including *CustomPlasmaReaction* objects defining the rate constants of transport losses or gains of the adjacent phases. Regarding the *Electrode* boundaries the *PlasmaInterface* is coupling the *ExtensibleReactor* containing the *PlasmaSolution* with a *ConstPressureMoleReactor* containing a *fixed-stoichiometry* phase representing the solid electrode phase. On the other hand, the gas-plasma interface for plasma-gas mixtures modeling can be represented by a *PlasmaInterface* as well connecting two *ExtensibleReactors* for the two *PlasmaSolutions*. Even if it does not include charged particles, the choice of representing the gas through a *PlasmaSolution* allows the inclusion non-equilibrium reactions that may occur between the transported species.

3. Validation results

The code validation has been performed against the ZDPlasKin solver [48] on three chemistries. To ensure the comparability of the results, the same conditions available in the model adopted by ZDPlasKin were replicated in SPPARK. The first chemistry refers to an N_2 discharge under a simple custom power pulse solicitation. The second chemistry refers to an Ar plasma ignited under a continuous (DC) voltage signal, coupled to the chemistry through a simple circuit model, considering a multicomponent EBE solution and charged species losses due to ambipolar diffusion. The third chemistry, referring to a CH_4 discharge, is ultimately presented to introduce an example to further discuss on the potential differences

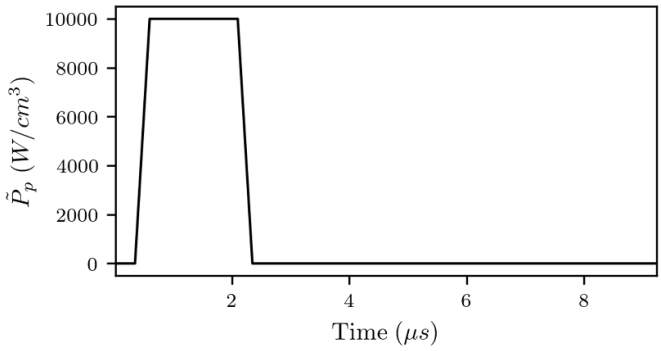

Figure 5. Power density signal provided to the simulation.

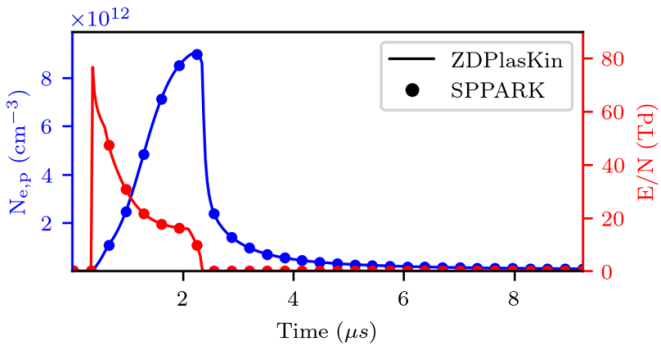

Figure 6. Electron number density (blue) and reduced electric field (red) results comparison between ZDPlasKin (continuous line) and SPPARK (dots) simulations for a pure N_2 plasma at a constant temperature of 298.15 K and 1 bar of pressure.

in non-isothermal plasma-chemistry simulations when adopting a rigorous gas thermodynamic approach.

3.1. N_2 discharge

A homogeneous ($\varphi = 1$), closed PSR with a volume of 1 m^3 was chosen to represent the discharge domain. The adopted chemistry set represents a N_2 discharge at 1 bar and is freely available in the ZDPlasKin website. The gas temperature was set constant at 298.15 K. The electron solicitation was provided as deposited power density (figure 5) under the LFA model as additional ODEs cannot be included in the ZDPlasKin equation system.

In figure 6 the results on the electron density and reduced electric field computed by SPPARK are shown against the same values obtained by ZDPlasKin. Figure 7 shows the computations of both solvers on heavy species number densities. The results show a good agreement between the two solvers computations. The maximum relative errors between the two have been calculated and are shown in figure 8 proving the almost exact equivalence in the two different solvers. Replicating the same approach, the code has been tested on multiple cases with varying power signals, pressure and temperatures showing a good agreement between results (figures 9–11). Since SPPARK employs an adaptive time-stepping scheme both for computation and for storing results, while ZDPlasKin restricts output to user-defined time instants,

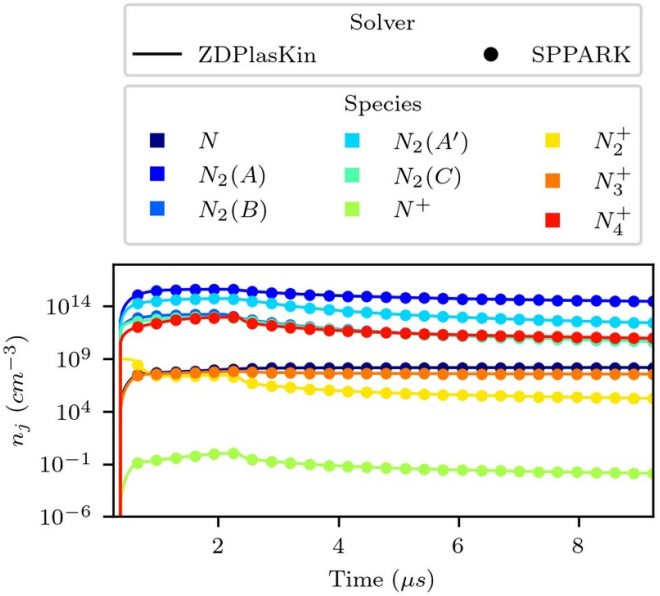

Figure 7. Heavy particles number densities results comparison between ZDPlasKin (continuous line) and SPPARK (dots) simulations for a pure N_2 plasma at a constant temperature of 298.15 K and 1 bar of pressure.

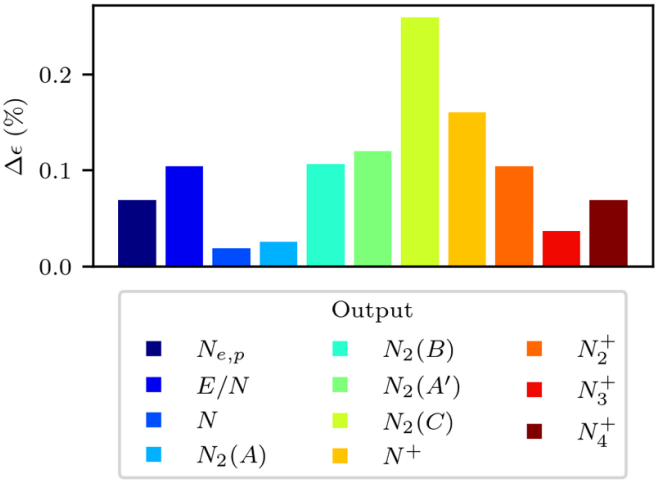

Figure 8. Maximum relative error (in percent) between the SPPARK and ZDPlasKin computation.

a time interpolation of the SPPARK simulation results was performed to enable a direct comparison at the same output times. It is worth noting that the minor discrepancies observed between the results may be attributed to this interpolation procedure. The SPPARK executions took an average of 3 min and 31.12 s whilst the ZDPlasKin executions took 1 min and 2.81 s.

3.2. Ar discharge

A plasma chemistry set comprising charged particles transport loss mechanisms due to ambipolar diffusion in an Ar plasma is available for ZDPlasKin. The considered plasma system represents a homogeneous Ar plasma at a pressure

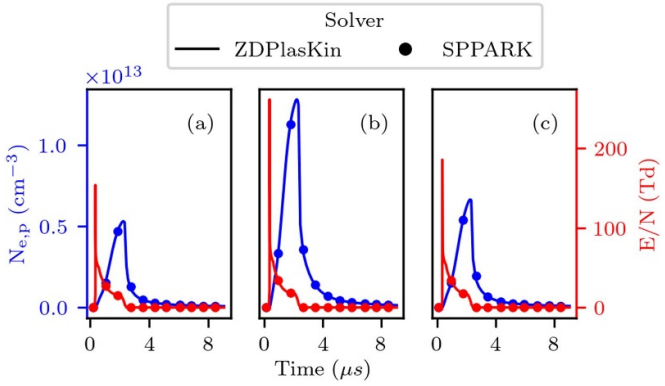

Figure 9. Electron number density (blue) and reduced electric field (red) results comparison between ZDPlasKin (continuous line) and SPPARK (dots) simulations for a pure N_2 plasma at: (a) a constant temperature of 298.15 K, 2 bar of pressure and 10^4 W cm^{-3} of peak deposited power density; (b) a constant temperature of 500 K, 1 bar of pressure and 10^4 W cm^{-3} of peak deposited power density; (c) a constant temperature of 298.15 K, 1 bar of pressure and $7.5 \cdot 10^3$ W cm^{-3} of peak deposited power density.

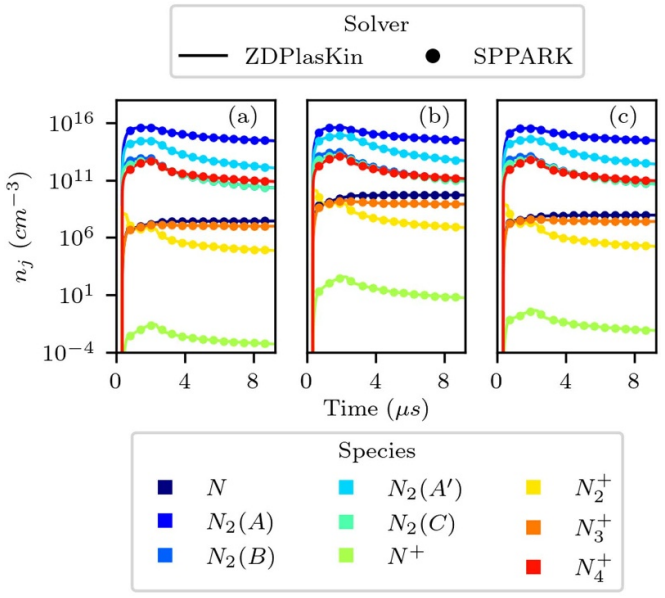

Figure 10. Heavy particles number densities results comparison between ZDPlasKin (continuous line) and SPPARK (dots) simulations for a pure N2 plasma at: (a) a constant temperature of 298.15 K, 2 bar of pressure and 10^4 W cm^{-3} of peak deposited power density; (b) a constant temperature of 500 K, 1 bar of pressure and 10^4 W cm^{-3} of peak deposited power density; (c) a constant temperature of 298.15 K, 1 bar of pressure and $7.5 \cdot 10^3$ W cm^{-3} of peak deposited power density.

of 100 torr and a constant temperature of 300 K in a cylindrical reactor having a radius (r) of 4 mm and a gap (d) between electrodes of 4 mm. The electron solicitation was provided in the form of reduced electric field values by coupling a simple circuit model composed of a DC voltage generator and a series of a ballast resistor and a plasma resistance representing the discharge, while neglecting the voltage drop across the sheaths, to the plasma-chemistry model. Even

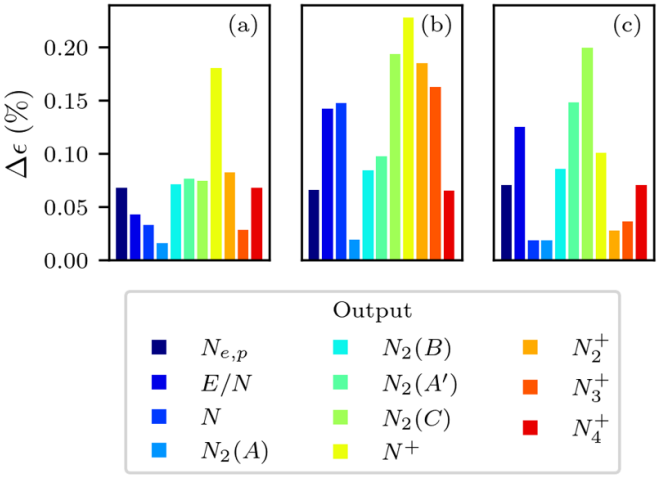

Figure 11. Maximum relative error (in percent) between the SPPARK and ZDPlasKin computations at: (a) a constant temperature of 298.15 K, 2 bar of pressure and 10^4 W cm^{-3} of peak deposited power density; (b) a constant temperature of 500 K, 1 bar of pressure and 10^4 W cm^{-3} of peak deposited power density; (c) a constant temperature of 298.15 K, 1 bar of pressure and $7.5 \cdot 10^3$ W cm^{-3} of peak deposited power density.

if the circuit model might not be the best representation of a plasma-electrical behavior, it has been implemented to further compare SPPARK computations against ZDPlasKin. The DC voltage signal (U) was set at 1 kV with a ballast resistor (R) of 1 kΩ. The plasma resistance was calculated through the plasma conductivity ($\sigma \approx N_{e,p} e \mu_e$) accordingly with the time-evolving electron density and mobility. In SPPARK, the circuit is coupled with the chemistry by providing the circuit net to an *ExtensibleIdealGasMoleReactor* object from Cantera, adapted to explicitly solve the circuit voltage and current equations and the reduced electric field has been computed from the voltage drop across the plasma resistance. This feature allows to generalize the applicability of the approach to an arbitrary circuit net which is automatically translated from its components and circuit nodes definition to the constitutive circuit equations. To ensure a smooth evolution of the plasma conductivity in time, the time step has been limited to a maximum of 1 ns. In ZDPlasKin the coupling has been performed as implemented in the in the reference example as expressed in equation (14):

$$\begin{cases} J = e\left(\pi r^2\right) N_e v_d \\ \left(\frac{E}{N}\right)_{test} = \frac{1}{N} \frac{U}{d + \frac{RJ}{10^{-17} E^{(t)} + 10^{-99}}} \\ \frac{E}{N}^{(t+1)} = 0.5\left[\left(\frac{E}{N}\right)_{test} + \left|\left(\frac{E}{N}\right)_{test}\right|\right] \end{cases} \tag{14}$$

where J is the electron current (A), e is the electron charge (C), N_e is the electron number density $\left(\mathrm{cm}^{-3}\right)$, v_d is the electron drift velocity, N is the neutral particles density $\left(\mathrm{cm}^{-3}\right)$, r and d are respectively the discharge radius and diameter (cm), $E^{(t)}$ and $E^{(t+1)}$ are respectively the electric field at the current time-step is the electric field at the next time-step $\left(\mathrm{V\,cm}^{-1}\right)$.

The ambipolar diffusion losses were included using two different approaches for ZDPlasKin and SPPARK. The

ZDPlasKin model treats these as homogeneous phase reactions leading to the production of wall-attached species. In SPPARK they were included as plasma-boundary interactions (described in section 2.3), considering the whole external surface of the plasma phase as available for the charged species losses. To better clarify how such reactions are included in SPPARK the example for the ambipolar diffusion losses is provided (equation (15)),

$$\begin{cases} \Lambda = \left(\frac{2.405}{r}\right)^2 + \left(\frac{3.1410}{d}\right)^2 \\ \nu = 1.52\frac{760}{p}\frac{T_g}{273.15}\frac{T_e}{11600}\Lambda \\ k(T_g, T_e, p) = \nu\frac{V}{A}\frac{10^3}{S_d N_a} \end{cases} \tag{15}$$

where V is the reactor volume (m^3), A is the total external surface (m^2), S_d is the surface active-sites density ($kmol\,m^{-2}$), N_a is the Avogadro constant, T_g is the gas temperature (K), T_e is the electron temperature (K), p is the gas pressure (Torr) and k is the rate constant for the ambipolar diffusion losses ($cm^3\,s^{-1}$). This expression can be directly implemented in a Python function giving the k value as a *return* to be passed as an argument to the *PlasmaCustomReaction* object representative of the ambipolar diffusion loss reaction.

To ensure the full comparability of the models, a two-step of comparison was performed. The first step concerned a homogeneous phase model, obtained by neglecting the transport losses by ambipolar diffusion. In the second one, the ambipolar diffusion loss mechanisms were included to evaluate the equivalence of the two approaches.

In figures 12 and 13 the computed electron density together with the reduced electric field values and the heavy species number densities obtained in the two simulations (A—no-ambipolar diffusion losses and B—including the ambipolar diffusion losses) are respectively shown. In both cases, the results show a good agreement (figure 14) between ZDPlasKin and SPPARK with the discrepancies possibly due to the time interpolation of the results in SPPARK (as in section 3.1) and to the different approach in the circuit to chemistry coupling. The simulation in SPPARK took 4 min and 49.13 s to execute for the case without ambipolar diffusion losses and 5 min and 24.41 s for the case including ambipolar diffusion losses whilst in ZDPlasKin tool 18.78 s and 27.51 s respectively.

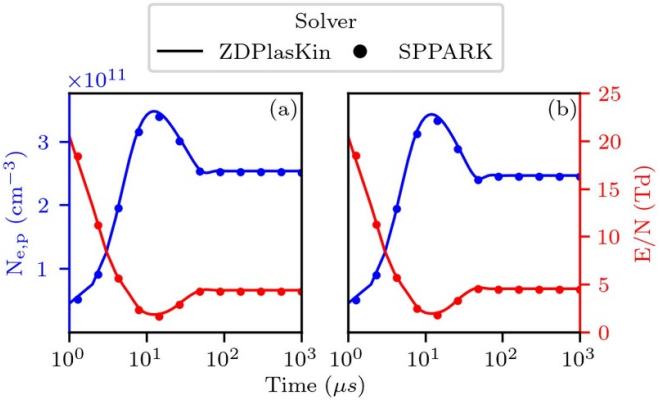

Figure 12. Electron number density (blue) and reduced electric field (red) results comparison between ZDPlasKin (continuous line) and SPPARK (dots) simulations for a pure Ar plasma at a constant temperature of 300 K and 100 torr of pressure, neglecting (a) and including (b) ambipolar losses in the chemistry set.

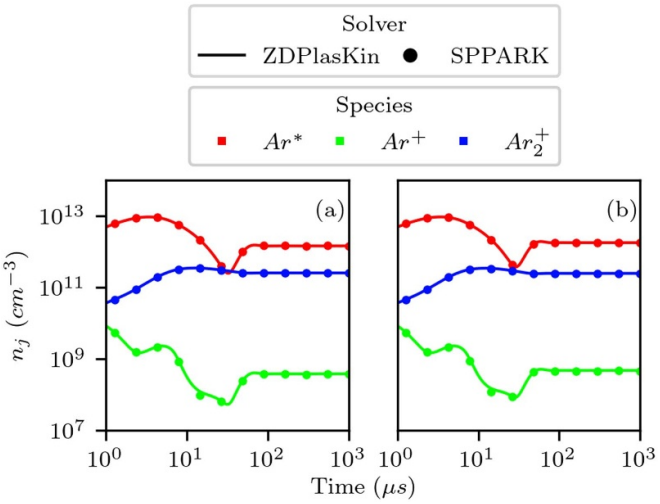

Figure 13. Heavy particles number densities results comparison between ZDPlasKin (continuous line) and SPPARK (dots) simulations for a pure Ar plasma at a constant temperature of 300 K and 100 torr of pressure, neglecting (a) and including (b) ambipolar losses in the chemistry set.

3.3. CH_4 discharge

In this example, a homogeneous PSR with free-to-variate temperature is used to simulate the dissociation of methane in a plasma discharge. A power density of 75 W mm^{-3} having the same shape of the signal in figure 5 is used as electron solicitation in a pure methane mixture at 298.15 K and 1 bar. The adopted chemistry set is composed of five species (e^-, CH_4, CH_3, H and CH_4^+) reacting through the reactions described in table 1. Being the chemistry set so approximate, the simulation purpose is not to present accurate results on methane dissociation in a plasma discharge, but rather to highlight the need of a proper species thermodynamic description for temperature-evolving systems.

In both the SPPARK and ZDPlasKin models, the species thermodynamic data has been obtained from NASA7 polynomials as provided by the GRI-Mech 3.0 mechanism [59]. Being based on Cantera, SPPARK can directly accept the polynomials coefficients in its configuration file. The ZDPlasKin model has been featured with user-defined functions to use the NASA7 polynomials data to compute the ratio of specific heats of the evolving gas mixture.

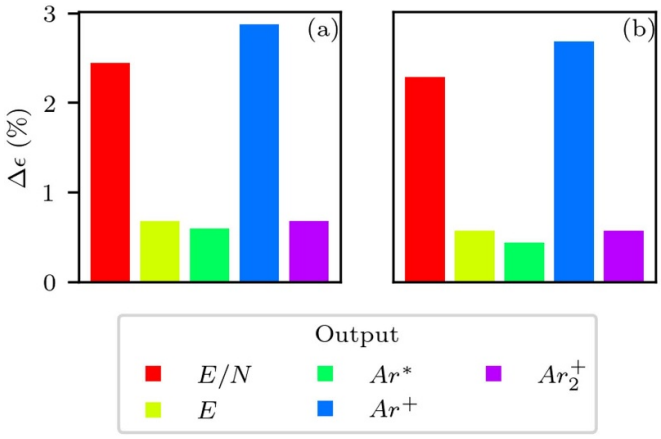

Figure 14. Maximum relative error (in percent) between the SPPARK and ZDPlasKin computations at a constant temperature of 300 K and 100 torr of pressure, neglecting (a) and including (b) ambipolar losses in the chemistry set.

Table 1. Chemical reactions included in the methane chemistry set. The rate constants are expressed in $cm^3\ s^{-1}$ with $\boldsymbol{f(\sigma)}$ being obtained through the Bolsig+ EEDF computation and $\boldsymbol{T_g}$ being the gas temperature expressed in K.

Id	Equation	Rate constant
1	$e^- + CH_4 \Rightarrow 2e^- + CH_4^+$	$f(\sigma)$ [60]
2	$e^- + CH_4 \Rightarrow e^- + CH_3 + H$	$f(\sigma)$ [61]
3	$e^- + CH_4^+ \Rightarrow CH_3 + H$	$f(\sigma)$ [62]
4	$CH_3 + H \Rightarrow CH_4$	$k_{Troe}\,(T_g)$ [59]

In table 1, k_{Troe} is defined as in equation (16):

$$\begin{cases} k_\infty = 2.31\cdot 10^{-8} T_g^{-0.534} exp\left(-\dfrac{269.75}{T_g}\right) \\ k_0 = 1.44\cdot 10^{-14} T_g^{-4.74} exp\left(-\dfrac{1227.98}{T_g}\right) \\ F_c = (1-A)\,exp\left(-\dfrac{T_g}{T_3}\right) + A\,exp\left(-\dfrac{T_g}{T_1}\right) + exp\left(-\dfrac{T_2}{T_g}\right) \\ C = -0.4 - 0.67\log_{10}F_c \\ N = 0.75 - 1.27\log_{10}F_c \\ P_r = \frac{k_o[M]}{k_\infty} \\ f_1 = \dfrac{\log_{10}P_r + C}{N - 0.14\,(\log_{10}P_r + C)} \\ F(T_g, P_r) = 10^{\frac{\log_{10}F_c}{1+f_1^2}} \\ k_{Troe} = k_\infty \left(\dfrac{P_r}{1+P_r}\right) F(T_g, P_r) \end{cases} \tag{16}$$

where $A = 0.783$, $T_1 = 2941\ K$, $T_2 = 6964\ K$, $T_3 = 74\ K$, $[M]$ is the sum of number densities of any neutral species such that $k_0\,[M]$ and k_∞ are respectively the low-pressure and the high-pressure limits of the rate constant $\left(cm^3\,s^{-1}\right)$.

To ensure the equivalence of the two solvers implementation of gas heating due to electron-neutral elastic collisions, a first simulation neglecting reaction enthalpies has been performed. The agreement between the two approaches begins to diminish as the energy contribution of reaction 4 of table 1 is considered in the model. In fact, to the best of Authors' knowledge, the enthalpy of reaction must be provided as a constant value to the ZDPlasKin chemistry set input file, whilst it should be changing across the gas temperature spectrum accordingly with the enthalpy of formation of the species it features. This represents an approximation when dealing with large gas temperature ranges in the simulation. To better clarify this concept the values of internal energy of reaction for each CH_3 and H recombination to CH_4 occurring is presented in figure 15. In figure 16 the two simulations relative differences in the gas temperature computation are presented together with the gas temperature change in time due to reaction 4. From figure 16 it is noticeable how the ZDPlasKin and SPPARK discrepancy is related to the introduction of the heat released by reaction 4. It is worth noticing that the discrepancy would increase with a larger number of temperature influencing reactions. For the 2 comparisons the average computation time for SPPARK is registered to be of 4 min and 2.1 s whilst the ZDPlasKin execution took 8 min and 22.80 s.

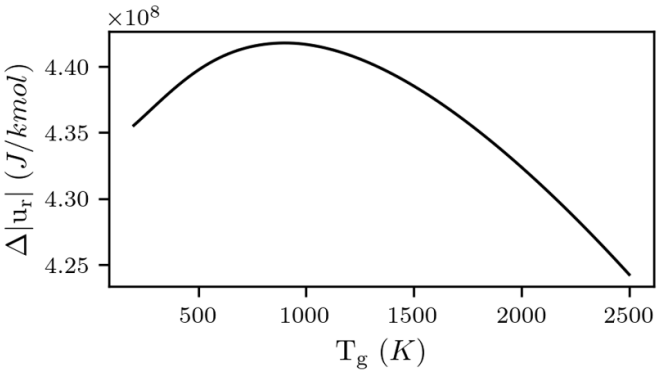

Figure 15. Internal energy of reaction for CH_3 and H recombination to CH_4.

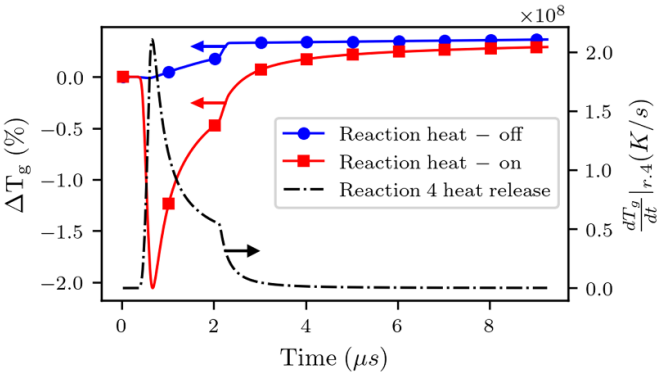

Figure 16. Comparison of the gas temperature time-evolution in the two simulations having the internal energy of reaction 4 excluded (blue) and included (red) in the simulation together with the heat release of reaction 4 (black).

4. Conclusions

Due to their potential to enhance the environmental sustainability of chemical process, non-equilibrium plasmas are gaining increasing interest in this technological field. Being characterized by multi-physical complex mechanisms, the study of plasma-chemistry processes often requires the application of numerical models to gain detailed insights into their founding principles. In this context, 0D plasma-chemistry solvers allow to focus on detailed chemistries limiting the simulations computational time. To ensure full customization and flexibility of application of a plasma-chemistry solver, it should be able to accurately consider both the electronic and thermo-chemical effects. SPPARK, a novel plasma chemistry solver based on Cantera and Bolsig+, has been developed. The solver makes use of the formalism and robustness of Cantera's models in thermo-chemical simulations together with the completeness of the description of the electronic kinetics of the Bolsig+ model, coupling them through many state-of-the-art models for the numerical representation of plasma effects in a plasma-gaseous system allowing users to represent many different plasma-chemical processes. The validity of the code has also been proven by comparison of its simulations results against the simulations obtained through the state-of-the-art solver ZDPlasKin on two different chemistry-sets on multiple validation cases. In addition, a test case on a simple methane splitting chemistry has been presented to extend the comparison of the two solvers to models characterized by time-evolving gas temperatures. Due to the different approaches in species and reactions thermodynamics representations, the results show relevant differences in the gas temperature results which could rapidly build up when implementing more complex reaction schemes.

Data availability statement

All data that support the findings of this study are included within the article (and any supplementary files).

Acknowledgment

The PhD scholarships of the author Marchetti, A. was funded by Nuovo Pignone Tecnologie Srl. and by the European Union—NextGenerationEU through the Italian Ministry of University and Research under PNRR—Mission 4 Component 2, Investment 3.3 'Partnerships extended to universities, research centres, companies and funding of basic research projects' D.M. 352/2021—CUP J33C22001480009. The authors are thankful to Elkid Cobani for the constructive discussions.

ORCID iDs

Andrea Marchetti 0009-0008-0887-9191
Romolo Laurita 0000-0003-1744-3329
Matteo Gherardi 0000-0001-6995-6754

References

[1] De Bie C, Verheyde B, Martens T, van Dijk J, Paulussen S and Bogaerts A 2011 Fluid modeling of the conversion of methane into higher hydrocarbons in an atmospheric pressure dielectric barrier discharge *Plasma Process. Polym.* **8** 1033–58
[2] Wnukowski M 2023 Methane pyrolysis with the use of plasma: review of plasma reactors and process products *Energies* **16** 6441
[3] Yuan X, Sun J, Ma Y, Wang Y, Liu B, Cai Y, Yong X and Tu X 2024 A kinetic study of nonthermal plasma pyrolysis of methane: insights into hydrogen and carbon material production *Chem. Eng. J.* **499** 156396
[4] Li T, Rehmet C, Cheng Y, Jin Y and Cheng Y 2017 Experimental comparison of methane pyrolysis in thermal plasma *Plasma Chem. Plasma Process.* **37** 1033–49
[5] An H, Cheng Y, Li T, Li Y and Cheng Y 2018 Numerical analysis of methane pyrolysis in thermal plasma for selective synthesis of acetylene *Fuel Process. Technol.* **172** 195–9
[6] Daghagheleh O, Schenk J, Zarl M A, Lehner M, Farkas M and Zheng H 2023 Feasibility of a plasma furnace for methane pyrolysis: hydrogen and carbon production *Energies* **17** 167
[7] Daghagheleh O, Schenk J, Zheng H, Zarl M A, Farkas M, Ernst D, Kieush L, Lehner M, Kostoglou N and Obenaus-emler R 2024 Optimizing methane plasma pyrolysis for instant hydrogen and high-quality carbon production *Int. J. Hydrog. Energy* **79** 1406–17
[8] Hazenberg T, van Dijk J and van Oijen J A 2023 Chemical flux analysis of low-temperature plasma-enhanced oxidation of methane and hydrogen in argon *Combust. Flame* **257** 113037
[9] Burger C M, Zhang A J, Xu Y, Hansen N and Ju Y 2023 Plasma-assisted chemical-looping combustion: low-temperature methane and ethylene oxidation with nickel oxide *J. Phys. Chem. A* **127** 789–98
[10] Sun J, Chen Q, Yang X and Koel B E 2019 Effects of non-equilibrium excitation on methane oxidation in a low-temperature RF discharge *J. Phys. D: Appl. Phys.* **53** 064001
[11] Ma T, Sun K, Meng L, Cheng P, Cheng Q and Li S 2024 Oxidation of lean methane by dielectric barrier discharge plasma and Mn–Ce catalyst *Chem. Eng. Process.—Process. Intensif.* **204** 109925
[12] Zhou M, Yang Z, Ren J, Zhang T, Xu W and Zhang J 2023 Non-oxidative coupling reaction of methane to hydrogen and ethene via plasma-catalysis process *Int. J. Hydrog. Energy* **48** 78–89
[13] Pourali N, Vasilev M, Abiev R and Rebrov E V 2022 Development of a microkinetic model for non-oxidative coupling of methane over a Cu catalyst in a non-thermal plasma reactor *J. Phys. D: Appl. Phys.* **55** 395204
[14] Maslova V, Nastase R, Veryasov G, Nesterenko N, Fourré E and Batiot-Dupeyrat C 2024 Current status and challenges of plasma and plasma-catalysis for methane coupling: a review *Prog. Energy Combust. Sci.* **101** 101096
[15] Maitre P-A, Long J, Bieniek M S, Bannerman M N and Kechagiopoulos P N 2022 Investigating the effects of helium, argon and hydrogen co-feeding on the non-oxidative coupling of methane in a dielectric barrier discharge reactor *Chem. Eng. Sci.* **259** 117731
[16] Wnukowski M, van de Steeg A W, Hrycak B, Jasiński M and van Rooij G J 2021 Influence of hydrogen addition on methane coupling in a moderate pressure microwave plasma *Fuel* **288** 119674
[17] Liu R, Hao Y, Wang T, Wang L, Bogaerts A, Guo H and Yi Y 2023 Hybrid plasma-thermal system for methane

conversion to ethylene and hydrogen *Chem. Eng. J.* **463** 142442
[18] Klimek A and Piercey D G 2024 Nitrogen fixation via plasma-assisted processes: mechanisms, applications, and comparative analysis—a comprehensive review *Processes* **12** 786
[19] Chen H, Yuan D, Wu A, Lin X and Li X 2021 Review of low-temperature plasma nitrogen fixation technology *Waste Dispos. Sustain. Energy* **3** 201–17
[20] Manaigo F, Bogaerts A and Snyders R 2024 Study of a gliding arc discharge for sustainable nitrogen fixation into NOx *2024 IEEE Int. Conf. on Plasma Science (ICOPS)* (IEEE) pp 1
[21] Aceto D, Ambrico P F and Esposito F 2024 Air cold plasmas as a new tool for nitrogen fixation in agriculture: underlying mechanisms and current experimental insights *Front. Phys.* 1455481 **12**
[22] Lamichhane P, Pourali N, Rebrov E V and Hessel V 2024 Energy intensified nitrogen fixation through fast modulated gas discharge from pyramid-shaped micro-electrode *Plasma Chem. Plasma Process.* **44** 1369–92
[23] Gao H, Wang G, Huang Z, Nie L, Liu D, Lu X, He G and Ostrikov K K 2023 Plasma-activated mist: continuous-flow, scalable nitrogen fixation, and aeroponics *ACS Sustain. Chem. Eng.* **11** 4420–9
[24] Zhao X and Tian Y 2023 Sustainable nitrogen fixation by plasma-liquid interactions *Cell Rep. Phys. Sci.* **4** 101618
[25] Muzammil I, Lee D H, Dinh D K, Kang H, Roh S A, Kim Y-N, Choi S, Jung C and Song Y-H 2021 A novel energy efficient path for nitrogen fixation using a non-thermal arc *RSC Adv.* **11** 12729–38
[26] Centi G, Perathoner S and Papanikolaou G 2021 Plasma assisted CO_2 splitting to carbon and oxygen: a concept review analysis *J. CO2 Util.* **54** 101775
[27] Burghaus H, Kaiser C F, Fasoulas S and Herdrich G 2023 Influence of specific energy inhomogeneity on the CO_2 splitting performance in a high-power plasma jet *Vacuum* **217** 112500
[28] Scurtu A, Ticoș D, Mitu M L, Diplașu C, Udrea N and Ticoș C M 2023 Splitting CO_2 in intense pulsed plasma jets *Int. J. Mol. Sci.* **24** 6899
[29] Liu Z, Zhou W, Xie Y, Liu F, Fang Z, Zhang G and Jin W 2023 Highly effective CO_2 splitting in a plasma-assisted membrane reactor *J. Membr. Sci.* **685** 121981
[30] Renninger S, Lambarth M and Birke K P 2020 High efficiency CO_2-splitting in atmospheric pressure glow discharge *J. CO2 Util.* **42** 101322
[31] Meng G, Xia L, Cheng Y and Yin Z 2023 AC-driven atmospheric pressure glow discharge co-improves conversion and energy efficiency of CO_2 splitting *J. CO2 Util.* **70** 102447
[32] Mahdikia H, Brüser V, Schiorlin M and Brandenburg R 2023 CO_2 dissociation in barrier corona discharges: effect of elevated pressures in CO_2/Ar mixtures *Plasma Chem. Plasma Process.* **43** 2035–63
[33] Renninger S, Stein J, Lambarth M and Birke K P 2022 An optimized reactor for CO_2 splitting in DC atmospheric pressure discharge *J. CO2 Util.* **58** 101919
[34] Faingold G, Kabour R, Shen S and Lefkowitz J K 2024 Reforming of ammonia and ammonia-air mixtures in a homogenous plasma reactor: parametric study of hydrogen yields *Int. J. Hydrog. Energy* **73** 856–67
[35] Zhang X and Cha M S 2024 Ammonia cracking for hydrogen production using a microwave argon plasma jet *J Phys D Appl Phys* **57** 065203
[36] Bang S, Snoeckx R and Cha M S 2023 Kinetic Study for Plasma Assisted Cracking of NH_3 : approaches and Challenges *J. Phys. Chem. A* **127** 1271–82
[37] Zhang X and Cha M S 2024 Optimizing ammonia cracking in microwave argon plasma: temperature control and ammonia delivery *Chem. Eng. J.* **496** 154289
[38] Zhang X, Shan Y, Sun Z, Pan H, Zhang L, Zhu Z, Feng F, Han J and Li K 2024 Mechanism of plasma chemistry in CO_2 hydrogenation using a dielectric barrier discharge reactor *Plasma Process. Polym.* **21** 2300215
[39] Ullah N, Su M, Yang Y and Li Z 2023 Enhanced CO_2 hydrogenation to light hydrocarbons on Ni-based catalyst by DBD plasma *Int. J. Hydrog. Energy* **48** 21735–51
[40] Li K, Teng P, Fei R, Lu Z, Zhang L and Zhang X 2025 Reaction mechanism of plasma chemistry in CO_2 hydrogenation: the effect of CO_2/H_2 ratio *J Electrost.* **134** 104017
[41] Wang L, Yi Y, Guo H and Tu X 2018 Atmospheric pressure and room temperature synthesis of methanol through plasma-catalytic hydrogenation of CO_2 *ACS Catal.* **8** 90–100
[42] Chen Y, Peng Y, Qian M, Liu S, Zhang J and Wang D 2022 A zero-dimensional model for atmospheric non-thermal plasma CO_2 hydrogenation: insights into the reaction mechanism *Jpn J. Appl. Phys.* **61** 086001
[43] Liu M, Yi Y, Wang L, Guo H and Bogaerts A 2019 Hydrogenation of carbon dioxide to value-added chemicals by heterogeneous catalysis and plasma catalysis *Catalysts* **9** 275
[44] Fridman A 2008 *Plasma Chemistry* 9780521847353 pp 1–978
[45] Popov N A 2011 Fast gas heating in a nitrogen–oxygen discharge plasma: i. Kinetic mechanism *J. Phys. D: Appl. Phys.* **44** 285201
[46] Mintoussov E I, Pendleton S J, Gerbault F G, Popov N A and Starikovskaia S M 2011 Fast gas heating in nitrogen–oxygen discharge plasma: II. Energy exchange in the afterglow of a volume nanosecond discharge at moderate pressures *J. Phys. D: Appl. Phys.* **44** 285202
[47] Hagelaar G J M and Pitchford L C 2005 Solving the Boltzmann equation to obtain electron transport coefficients and rate coefficients for fluid models *Plasma Sources Sci. Technol.* **14** 722–33
[48] Pancheshnyi S, Eismann B, Hagelaar G and Pitchford L 2008 ZDPlasKin
[49] van Dijk J, Peerenboom K, Jimenez M, Mihailova D and van der Mullen J 2009 The plasma modelling toolkit plasimo *J. Phys. D: Appl. Phys.* **42** 194012
[50] Cheng L, Barleon N, Cuenot B, Vermorel O and Bourdon A 2022 Plasma assisted combustion of methane-air mixtures: validation and reduction *Combust. Flame* **240** 111990
[51] Shao X, Lacoste D A and Im H G 2024 ChemPlasKin: a general-purpose program for unified gas and plasma kinetics simulations *Appl. Energy Combust.Sci.* **19** 100280
[52] Shane K 2022 CRANE (available at: https://github.com/lcpp-org/crane)
[53] Goodwin D G, Moffat H K, Schoegl I, Speth L R and Weber B W 2024 Cantera: an object-oriented software toolkit for chemical kinetics, thermodynamics, and transport processes
[54] Lieberman M A and Lichtenberg A J 2005 *Principles of Plasma Discharges and Materials Processing* 2nd edn (Wiley) pp 1–757
[55] Heijkers S, Aghaei M and Bogaerts A 2020 Plasma-based CH_4 conversion into higher hydrocarbons and H_2 : modeling to reveal the reaction mechanisms of different plasma sources *J. Phys. Chem. C* **124** 7016–30
[56] Morais E, Delikonstantis E, Scapinello M, Smith G, Stefanidis G D and Bogaerts A 2023 Methane coupling in nanosecond pulsed plasmas: correlation between temperature and pressure and effects on product selectivity *Chem. Eng. J.* **462** 142227

[57] Grubert G K, Becker M M and Loffhagen D 2009 Why the local-mean-energy approximation should be used in hydrodynamic plasma descriptions instead of the local-field approximation *Phys. Rev. E* **80** 036405
[58] Alves L L and Tejero-del-caz A 2023 Charged-particle transport models for global models *Plasma Sources Sci. Technol.* **32** 054003
[59] Gregory P S *et al* GRI-Mech Home Page (available at: www.me.berkeley.edu/gri_mech/)
[60] Lindsay B and Mangan M 2003 *Interactions of Photons and Electrons with Molecules* vol 17C (Springer)
[61] Bouwman D, Martinez A, Braams B J and Ebert U 2021 Neutral dissociation of methane by electron impact and a complete and consistent cross section set *Plasma Sources Sci. Technol.* **30** 075012
[62] Braams B J and Chung H-K 2014 *Tomic and Plasma-Material Interaction Data for Fusion. V. 16* (IAEA)